ADVANCED MATERIALS TECHNOLOGIES
www.advmattechnol.de

4D Printing of Supramolecular Liquid Crystal Elastomer Actuators Fueled by Light

*Sean J. D. Lugger, Lorena Ceamanos, Dirk J. Mulder, Carlos Sánchez-Somolinos, and Albert P. H. J. Schenning**

Recent years have seen major advances in the additive manufacturing of stimuli-responsive materials, also known as "4D printing," among which liquid crystal elastomers (LCEs) play an important role. However, during fabrication photo-crosslinking of the LCEs is required, but this step is time-consuming and efficient polymerization is challenging, especially in the case of light-responsive materials. In this work, the first light-fueled supramolecular LCEs suitable for the direct ink writing (DIW) of soft actuators are synthesized in which a photopolymerization step is not needed. With the responsive supramolecular material, 3D-printed objects are fabricated by exploiting the thermoreversible interplay of the hydrogen-bonding physical cross-links. After printing, the supramolecular LCE shows reversible shape changes in response to light and is capable of bending and lifting a load. Through the combined photothermal and photochemical contributions of the incorporated azobenzene, the actuators can be triggered both in air and water. The freedom provided by DIW allows for the printing of complex responsive objects, as demonstrated by fabricating re-entrant honeycomb and spiral director structures. This approach of printing light-responsive supramolecular soft actuators opens avenues toward the application of "smart" and sustainable materials for additive manufacturing without the requirement of photo-crosslinking.

1. Introduction

Among the potential applications of liquid crystal elastomer (LCE) based stimuli-responsive materials, the development of untethered soft actuators is one of the most attractive.[1–4] For example, in soft robotics,[5–8] as well as in microfluidics and biomimetic devices,[9,10] light-responsive LCE polymers containing photoactive molecules have been widely used.[11,12] The benefit of light as an untethered stimulus, in contrast to others such as temperature and humidity, is the spatial–temporal control, tunability, and straightforward application.[13–15] Therefore, efforts to develop light-driven actuators based on polymerizable LCE materials have become a well-established research topic, producing a valuable basis for transforming light into mechanical motion.[16,17] Azobenzene derivatives are currently the most prominent photo-switches in LCE actuators due to their ease of incorporation, and for enabling remotely controlled actuation with fast and reversible responses.[18,19] However, photopolymerization of liquid crystal (LC) materials is generally needed to obtain reversible shape changes.[20,21] This photoinduced cross-linking process is time-consuming, and efficient curing is challenging, which is even further impeded by the undesired isomerization of the azobenzene moieties.[22]

The potential of deploying physically cross-linked polymer actuators is an emerging research topic.[23–26] Because of the non-covalent nature of the physical cross-linking interactions, these supramolecular polymeric materials are often (re-)processable and photocuring is not required. In recent works, using light-addressable azobenzene-containing polyurethanes has allowed reversible photoinduced deformations.[27–29] This actuation behavior results from the *trans-cis* photoisomerization and the molecular disorder generated in the matrix upon illumination with light. While highlighting the versatility of physically cross-linked LCEs as an alternative for permanent cross-links in soft actuators, the processing of these materials is still limited.

Additive manufacturing techniques such as direct ink writing (DIW) is an attractive approach for fabricating LC-based objects, accommodating freedom in structural design and allowing for the fabrication of 3D stimuli-responsive materials.[30,31] This concept is also known as 4D printing, where the 3D printed material can change its shape or appearance in response to various

S. J. D. Lugger, D. J. Mulder, A. P. H. J. Schenning
Laboratory of Stimuli-responsive Functional Materials and Devices (SFD)
Department of Chemical Engineering and Chemistry
Eindhoven University of Technology
P.O. Box 513, Eindhoven MB 5600, The Netherlands
E-mail: a.p.h.j.schenning@tue.nl

L. Ceamanos, C. Sánchez-Somolinos
Instituto de Nanociencia y Materiales de Aragón (INMA)
Departamento de Física de la Materia Condensada
CSIC-Universidad de Zaragoza
Zaragoza 50009, Spain

C. Sánchez-Somolinos
CIBER Bioengineering, Biomaterials and Nanomedicine (CIBER-BBN)
Madrid 28029, Spain

A. P. H. J. Schenning
Institute for Complex Molecular Systems
Eindhoven University of Technology
P.O. Box 513, Eindhoven MB 5600, The Netherlands

The ORCID identification number(s) for the author(s) of this article can be found under https://doi.org/10.1002/admt.202201472.

DOI: 10.1002/admt.202201472

external stimuli.[32–36] To date, most of the LCE-based actuators fabricated via DIW are based on photopolymerizable inks and covalent cross-links, but the printing of light-responsive supramolecular LCE actuators has not been reported before.[37–39] However, in a particular example, photoswitchable actuators based on both dynamic covalent and supramolecular cross-links have been printed with DIW without photopolymerization being needed.[40] Hence, developing supramolecular LCE inks suitable for DIW with only dynamic physical cross-links for fabricating light-responsive actuators would be appealing. Only recently, we exploited the DIW of a temperature-responsive supramolecular ink for the facile fabrication of more sustainable soft actuators.[41]

In this work, we present a light-triggered, printable supramolecular ink based on a melt-processable polythiourethane (PTU) consisting of responsive LC and dynamic hydrogen-bonding segments. This thermoplastic material combines the thermoreversible nature of the supramolecular cross-links with the light-responsivity of the incorporated azobenzene photoswitches. After fabricating actuators by mechanical programming, DIW is used to generate light- and temperature-responsive supramolecular actuators without photo-crosslinking that demonstrate reversible shape changes. It is shown that the resulting supramolecular actuators can be addressed in either air or aqueous environments and are capable of performing mechanical work in response to light. The freedom in structural design and capabilities of mesogen alignment are demonstrated by DIW re-entrant honeycomb and spiral director structures with complex, reversible shape deformations.

2. Results and Discussion

2.1. Synthesis and Characterization of the Light-Responsive Supramolecular LCE

Light-driven response of the thermoplastic material is obtained by incorporating an azobenzene photoswitch, which is often used in conventional light-responsive LCE actuators (**Figure 1**a).[1,7] Inspired by the one-pot synthesis of supramolecular soft actuators reported earlier, a photoresponsive LCE based on segmented PTU has been synthesized.[42] By simply adding an azobenzene derivative (3 mol%) to diacrylate mesogens and reacting it with an excess of dithiol through a phosphine catalyzed nucleophilic thiol-Michael addition reaction, an azobenzene containing LC oligomer is yielded (Figure S1, Supporting Information). Subsequently, the thiol functionalized oligomer obtained is further reacted with an aliphatic diisocyanate and dithiol chain extender by a base-catalyzed addition reaction yielding a thermoplastic LCE with azobenzene moieties incorporated in the main chain. The synthesized polymer comprises alternating responsive and dynamic hydrogen-bonding segments, consisting of five and one repeating unit(s),

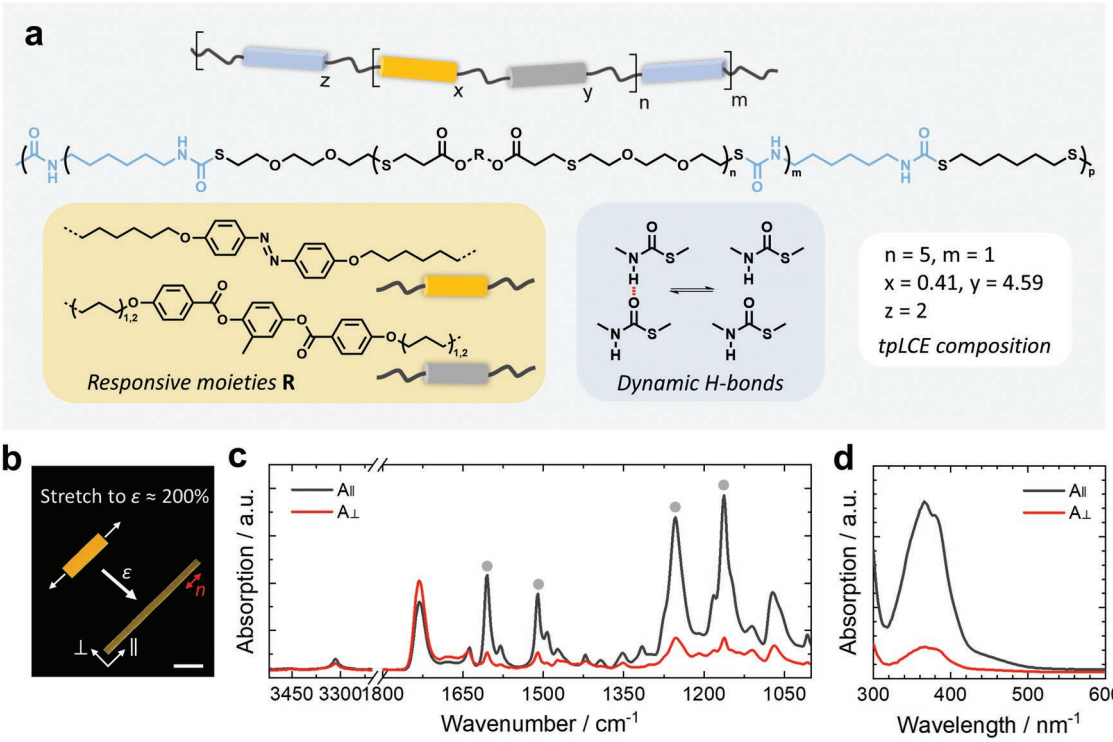

Figure 1. a) Schematic and molecular representation of the light-responsive thermoplastic LCE (tpLCE) and theoretical composition. The blue rectangles correspond to the chemical composition highlighted in blue. b) Stretching of compression-molded material, thereby inducing molecular order (*n*). The scale bar represents 1 cm. c) Linear polarized FT-IR and d) UV–vis spectra showing the absorption parallel (∥) and perpendicular (⊥) to the induced alignment of a stretched film. Gray dots in (c) indicate mesogen-specific vibrations.

respectively. Synthesis of the LCE ink was confirmed by gel permeation chromatography (GPC), indicated by the relatively high number-average molecular weight ($M_n \approx 77$ kg mol^{-1}) and low polydispersity index ($Đ = 1.97$; Figure S2, Supporting Information). In addition, the absence of thiol ($\tilde{\nu} \approx 2560$ cm^{-1}) and isocyanate ($\tilde{\nu} \approx 2270$ cm^{-1}) vibrations, as observed with Fourier-Transform infrared spectroscopy (FT-IR), are indicative of successful polymerization (Figure S3, Supporting Information). The formation of the PTU was further indicated by the presence of characteristic amine ($\tilde{\nu} \approx 3310$–3340 cm^{-1}) and carbonyl ($\tilde{\nu} \approx 1640$–1680 cm^{-1}) stretching bands.[43] Complete incorporation of the azobenzene derivative was confirmed with NMR spectroscopy. From the ^{1}H-NMR spectrum, the integrated ratio between the mesogenic and azobenzene moieties' aromatic protons corresponds to the initial molar ratio (Figure S4, Supporting Information). Complementary, diffusion-ordered NMR spectroscopy (DOSY) showed that the signals of azobenzene exhibit the same diffusion coefficient as the PTU (Figures S5 and S6, Supporting Information).[44]

Analyzing the thermal properties with differential scanning calorimetry (DSC) reveals that the LCE ink has a glass transition temperature (T_g) of −16 °C and an endothermic melting temperature (T_m) at 176 °C (Figure S7, Supporting Information). In polarized optical microscopy (POM), the material exhibits an isotropization temperature (T_i) from the ordered to disordered state over a temperature range of 60–80 °C, indicated by the loss in birefringence upon heating (Figure S8, Supporting Information). Upon cooling, the material became birefringent again at a considerably lower temperature with a large thermal hysteresis. We assume the T_i is not visible with DSC since this transition is too broad. The material's degradation temperature is determined to be 247 °C (1% weight loss) with thermogravimetric analysis (Figure S7, Supporting Information).[45] This reveals that the T_m is well below the thermal degradation onset of the thermoplastic LCE ink, allowing melt processing of the material with good thermal stability. The dynamic viscoelasticity of the thermoplastic ink was characterized by performing dynamic mechanical analysis (DMA) on compression-molded films (Figure S7, Supporting Information). The obtained thermogram showed a segmental α-relaxation transition at 5 °C, which is directly related to the T_g, and an accompanying shoulder at 37 °C.[46,47] Increasing the temperature further, a rubbery plateau was observed up to 120 °C, after which it transitions to the viscoelastic flow region, followed by the viscous flow. These results indicate the formation of physical cross-links within the supramolecular network at the rubbery plateau that can be reversibly broken at higher temperatures due to the dynamic nature of the hydrogen bonds, allowing for programming strain-induced orientation and melt-processing capabilities. Moreover, temperature-dependent FT-IR spectroscopy shows the thermoreversible formation and breaking of the dynamic hydrogen-bonding cross-links (Figure S9, Supporting Information). The mechanical properties of the LCE were studied with tensile testing at room temperature (Figure S7, Supporting Information). This measurement showed a relatively high tensile strength and elongation at break for dynamic LCEs of 7 MPa and 1250% strain, respectively, presumably due to the strong hydrogen-bonding interactions within the thiourethane (TU) segments.

Elongating a compression-molded supramolecular LCE film results in strain-induced molecular orientation (n) along the stretching direction (Figure 1b). With linearly polarized transmission FT-IR spectroscopy, the dichroism of manually stretched samples ($\varepsilon = 200\%$) was evaluated at different azimuthal angles (Figure 1c). Clear positive anisotropy is evident from the stacked spectra parallel ($\parallel$) and perpendicular ($\perp$) to the stretching direction, particularly for ether ($\tilde{\nu} \approx 1162$ and 1252 cm^{-1}) and benzene ($\tilde{\nu} \approx 1510$ and 1605 cm^{-1}) stretching vibrations originating from the mesogenic moieties.[48,49] As can be seen in the polar plots, there is a clear azimuthal dependence of the absorption over 360° attributed to the induced alignment (Figure S10, Supporting Information). From the dichroic ratio $D = A_\parallel / A_\perp$ derived from the IR spectra, one can calculate the order parameter $S = (D-1)/(D+2)$ of specific vibrations.[50] Typically, the molecular vibrational bands assigned to the benzene rings are used to determine the molecular orientation of the mesogens.[48,49] The stretched LCE exhibits an order parameter of $S = 0.59$ for the mesogens, indicating excellent strain-induced orientation (Supporting Information for details). In contrast, the vibrations assigned to the TU segment, i.e., the hydrogen-bonded amine ($\tilde{\nu} \approx 3315$ cm^{-1}) and carbonyl moieties ($\tilde{\nu} \approx 1638$ cm^{-1}), display less evident anisotropy. This difference in dichroism of the respective LC and TU moieties reveals that the latter experiences more hindrance during stretching, most likely due to hydrogen-bonding interactions present within these domains.[51,52] Optical characterization of the azobenzene photoswitches within the stretched film was performed with linear polarized ultraviolet–visible (UV–vis) absorption measurements (Figure 1d). Here, the absorption band at $\lambda = 365$ nm is characteristic of the azobenzene derivative and exhibits clear anisotropy,[39] which is also seen in the azimuthal plot (Figure S10, Supporting Information), with a high dichroic ratio corresponding to $S = 0.61$. As expected, this result is similar to the order parameter found for the mesogens with transmission infrared dichroism, given that both specific moieties are incorporated within the soft segment chains.

The supramolecular network dynamics are critical to programming mesogen alignment, enabling a macroscopic mechanical response upon applying an external stimulus. The dynamic behavior was explored with thermal stress–relaxation tests by stretching the samples to $\varepsilon = 100\%$ strain at temperatures from 100 to 150 °C (**Figure 2**a). It is clearly observed that the temperature-dependent stress relaxation decreases faster at higher temperatures, showing the hydrogen-bonding cross-links' dynamic character. Following from the characteristic relaxation time τ^* ($\sigma/\sigma_0 = e^{-1}$) at each respective temperature, the activation energy (E_a) was derived from the Arrhenius equation corresponding to 162 kJ mol^{-1} (Figure 2b and Supporting Information for details).[53] These results indicate that the dynamic character of the supramolecular network can be suppressed at lower temperatures, providing thermal stability, whereas at higher temperatures the dynamic character is promoted. When the material is exposed to an isostress ($\sigma = 10$ kPa) with increasing temperature, plastic flow is observed as the sample length dramatically enlarges, showing an onset temperature of ≈120 °C (Figure S11, Supporting Information). A minor enlargement around the T_i arises from the decrease in stiffness accompanying the ordered to disordered

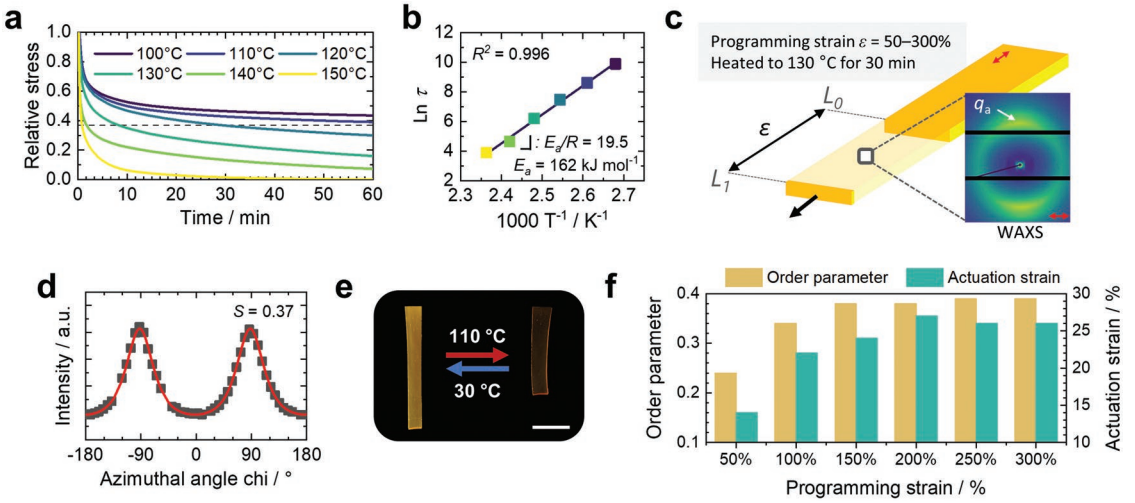

Figure 2. a) Thermal stress-relaxation of the supramolecular LCE as a function of time at temperatures from 100 to 150 °C with a constant strain (ε = 100%). The dashed line indicates the relaxation constant τ^* ($\sigma/\sigma_0 = e^{-1}$). b) Corresponding Arrhenius plot of the characteristic relaxation times (τ^*). c) Schematic representation of strain-induced alignment with varying strains and 2D X-ray diffractogram after programming (ε = 200%). The red arrows denote the alignment direction. d) Azimuthal profile at (q_a = 14.3–14.6 nm^{-1}) fitted with the Kratky method and e) thermal actuation of the actuator with a programming strain of ε = 200%. The scale bar in (e) represents 0.5 cm. f) The order parameter *S* obtained by WAXS and maximum thermal actuation at different programming strains (ε = 50–300%).

transition.[54] The distinct plastic flow indicates that the material exhibits little creep below this transition, allowing for stable actuation, while above this temperature, the material flows and mesogen alignment can be programmed by stretching.

Multiple compression-molded films were uniaxially stretched to different strains (ε = 50–300%) and subsequently heated to 130 °C for 30 min to program the strain-induced molecular alignment (Figure 2c).[42] This temperature is slightly above the onset temperature of plastic flow, where the hydrogen bonds are highly dynamic, enabling thermal rearrangement of the supramolecular cross-links. It should be noted that increasing the temperature further decreased the amount of strain the material could withstand before failing. The effect of different programming strains on the molecular orientation and actuation performance was studied by wide-angle X-ray scattering (WAXS; Figure 2d; Figures S12 and S13, Supporting Information) and thermal actuation measurements (Figure 2e), respectively. Comparing the obtained actuators of differing programming strains shows that the order parameter (S = 0.24–0.39) and actuation strain (ε_a = 14–27%) increase until 200% programming strain, after which both remain relatively constant (Figure 2f and Table S1, Supporting Information). The TU segments are more difficult to align than the LC segments due to the hydrogen-bonding interactions limiting the actuation strain (vide supra). Since the order parameter obtained with WAXS is averaged over the entire material, it is lower than derived from the linear-polarized FT-IR and UV–vis absorption measurements where only specific features are evaluated. The medium-angle X-ray scattering (MAXS) diffractograms of the programmed films showed that the diffraction peaks originating from the interdomain spacing at q_a = 0.28 nm^{-1} remained unchanged, which indicates that the microphase-separated morphologies are unaffected by the programming strain (Figure S14, Supporting Information).

2.2. Light Response of the Mechanically Programmed Supramolecular Actuator

A supramolecular soft actuator prepared with a programming strain of ε = 200% is used for photoactuation. The mechanically programmed LCE film bends toward the UV light source upon illumination (365 nm, 25 mW cm^{-2}) in air due to absorption of the azobenzene derivative (**Figure 3**; Video S1, Supporting Information). The azobenzene derivative undergoes light-induced isomerization from its rod-like *trans*-state to the bent *cis* isomer via the absorption of UV light (Figure 3a; Figure S15, Supporting Information).[1,20] Accompanying this *trans-cis* isomerization, the molecular order is disrupted due to conformational change of the isomer, inducing anisotropic contraction along the molecular director, thereby converting the absorbed light energy into mechanical work.[17,55] Due to the relatively high azobenzene content, a *cis-trans* gradient is created throughout the film, resulting in contraction of the exposed side leading to macroscopic bending (Figure S16, Supporting Information). After removing the UV light, the film partially unbends and remains in a temporarily stable deformation state arising from the photochemical effect of the light-induced *cis* population (Figure 3b,c). The partial unbending motion is most likely the consequence of a photothermal effect: UV light absorption of the azobenzene chromophores results in photothermal heating and contraction of the film at the irradiated side that reversibly expands into its temporary deformed state upon turning off the light. Photoinduced back isomerization of the *cis* azobenzene moieties can be immediately triggered by exposure to blue light (455 nm, 35 mW cm^{-2}), resulting in mechanical relaxation and large unbending deformations. However, the film completely unbends to its initial state only after turning off the blue light. This behavior can also be related to the light absorption of the azobenzene chromophores when exposed to

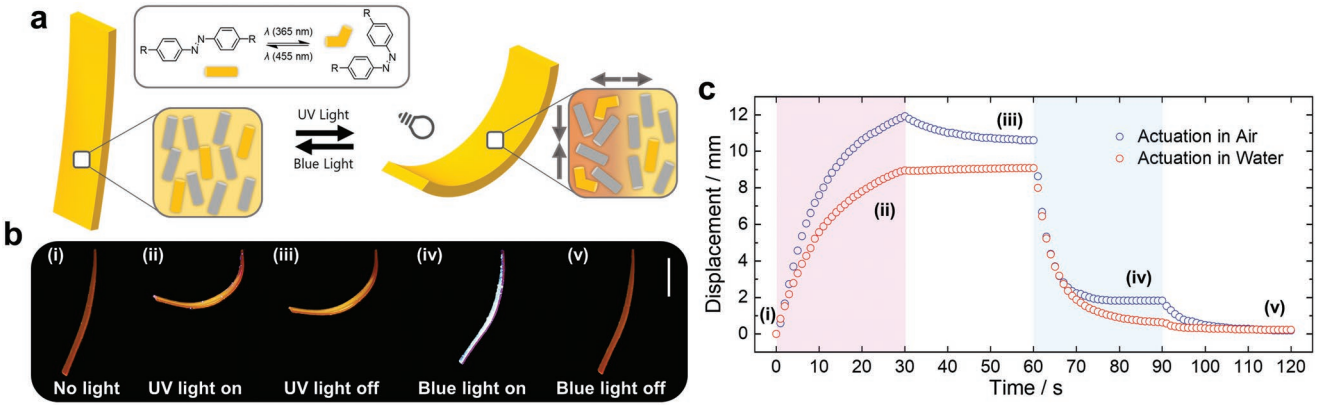

Figure 3. a) Light-induced *trans-cis* isomerization of the azobenzene derivative and schematic representation of the reversible light-driven bending motion arising from geometrical changes of the azobenzene moiety in response to light. The gray and orange rods represent the LC and light-responsive azobenzene moieties, respectively. Exposure to UV light leads to a light absorption (i.e., *cis-trans*) gradient in the film, indicated by the transition from dark to light orange color. b) Images of the photoactuation in air: i) actuator at room temperature before illumination; ii) UV light (25 mW cm^{-2}) induced bending motion; iii) temporary stable state of the actuator after removal of UV irradiation; iv) blue light (35 mW cm^{-2}) induced unbending motion; v) complete unbending to the initial state upon turning off the blue light. The actuator is illuminated from the left resulting in bending toward the light source. The scale bar represents 0.5 cm. c) Tip displacement of the actuator as a function of time in both air and water during UV (violet region) and blue (blue region) light illumination. The numbered regions correspond to the images in (b).

blue light resulting in photoinduced heating and contraction of the film, which expands to its initial state when the light is turned off.

Underwater actuation of the light-responsive thermoplastic LCE demonstrates almost no photothermal heating of the actuator since the generated heat is immediately lost into its surroundings, as indicated by the small unbending motions after removing both UV (20 mW cm^{-2}) and blue lights (29 mW cm^{-2}; Figure 3c; Video S2, Supporting Information). Additionally, the amplitude of deformation in water is smaller than in air since the same light intensities are used for both surroundings resulting in a higher intensity of incident light illuminating the film in air. These observations demonstrate that the light-responsive PTU LCE actuator operates both in air and water.

2.3. Direct Ink Writing and Light-Triggered Actuation of the Supramolecular LCEs

Given the responsive properties to temperature and light of the supramolecular LCE actuator films, this material was believed to be suitable for fabricating soft actuators through DIW. Typically, for printing LCE inks, the syringe is heated to around the T_i, while the print bed is maintained below this temperature to allow for the formation of molecular alignment.[56] In our case, the viscoelastic material was loaded into the printhead and heated to 200 °C, which is above its T_i and T_m, for 15 min to obtain a homogenous thermoplastic polymer melt. To achieve the required uniaxial molecular orientation, the viscosity of the melt is increased by setting the temperatures of the printhead and nozzle to 175 and 180 °C, respectively, allowing for shear and elongational flow during extrusion and filament deposition. At these printing temperatures, uniaxially aligned prints were obtained with printing speeds v_{nozzle} of 3–10 mm s^{-1}, 300 µm diameter nozzle, and the print substrate at room temperature (**Figure 4**a). As the molten material is extruded through the nozzle and deposited on the printing bed, it quickly cools and solidifies, thereby locking in the induced unidirectional alignment without additional polymerization

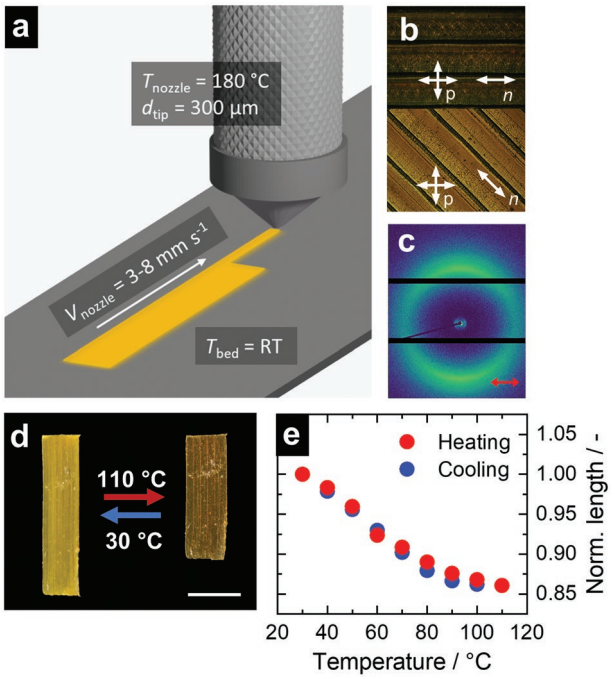

Figure 4. a) Scheme showing the fabrication of actuators through DIW. b) Optical microscopy images through cross-polarizers (p) with the printing direction (i.e., molecular director *n*) parallel (top) and at 45° (bottom). c) 2D X-ray diffractogram of the printed stripe showing orientationally arranged diffraction patterns orthogonal to the printing direction (red arrow). d) Photographs of the thermal actuation and corresponding e) actuation strain of the printed supramolecular LCE as a function of temperature upon cycling between 30 and 110 °C. The scale bar in (d) represents 0.5 cm.

steps. This interplay between the thermoplastic polymer melt and physically forming the cross-linked network is based on the thermoreversible nature of the hydrogen-bonding interactions. The material is printed on a substrate containing a sacrificial layer, e.g., poly(vinyl alcohol), which can be released to yield free-standing prints. After printing, the dark-bright (i.e., birefringence) state by rotating the printed sample between crossed polarizers with POM is indicative of uniaxial alignment, parallel to the printing direction (Figure 4b). WAXS further confirms the induced molecular alignment during printing, as can be seen by the typical diffraction pattern orthogonal to the printing direction with corresponding order parameter $S = 0.22$ (Figure 4c; Figure S17, Supporting Information). To verify the printed actuators' reversible response, it is heated to 110 °C, showing a 14% contraction that is completely recovered upon cooling to 30 °C (Figure 4d,e). A comparison of these results with the mechanically programmed actuators implies that the induced molecular order during printing corresponds to a programming strain of $\varepsilon = 50\%$ (Figure 2f; Table S1, Supporting Information).

Light-responsive, reversible actuation of the printed stripes is illustrated by sequential exposure to UV and blue lights (**Figure 5**). The macroscopic bending deformation of the printed actuator in both air and underwater is similar to the mechanically programmed actuator described previously (Figure 3): illumination with UV light (25 mW cm^{-2}) causes significant bending towards the light source that is completely recovered after exposure to blue light (35 mW cm^{-2}; Figure 5a,b). Accompanying the photoinduced isomerization, a slight increase in the film's surface temperature is observed that remains relatively constant during illumination (Figure S18, Supporting Information). Once the light is turned off, the film quickly cools to room temperature, causing it to slightly unbend into a temporarily stable state (vide supra). The partial unbending behavior after UV illumination is attributed to photothermal contributions, which is further strengthened by underwater actuation where this behavior is not observed since the heat is dissipated to the surrounding medium (Figure 5b). These combined observations and stable bending deformations indicate the photochemical nature of light-triggered actuation. The results also show that this supramolecular material is suitable for fabricating light-responsive printed actuators using DIW.

Using high-intensity UV illumination, it is possible to perform mechanical work and reversibly lift a load (1 g) in either air or underwater (Figure 5c,d). The weight also ensures contraction and expansion motions while preventing the undesired bending behavior during photoactuation, allowing to quantify the induced mechanical work. The printed actuator shows a contraction up to 14.4% upon exposure to UV light (220 mW cm^{-2}) in air, which remains constant during continuing illumination (Video S3, Supporting Information). When the UV light is turned off, the film rapidly expands back to an extent, followed by a gradual recovery reaching a remaining contraction of 3.9%. Accompanying the light-induced *trans-cis* isomerization, the film's temperature reaches almost 80 °C, which decreases to room temperature upon ceasing the light exposure (Figure S19, Supporting Information). These observations indicate a significant photothermal contribution to the light-induced weight-lifting actuation in air (10.5% contraction), corresponding to the actuation strain obtained with thermal actuation at 80 °C (11.0% contraction, Figure 4e). Subsequent blue light (15 mW cm^{-2}) illumination results in further recovery due to photoinduced back isomerization of the azobenzene moieties. However, only after switching off the blue light was there a complete recovery of the initial length, likely because of photothermal heating during illumination. Hence, both photothermal and photochemical effects determine the loaded actuator's contraction and work capacity in air. The extent of contraction underwater is significantly smaller than in air since photothermal heating of the film is suppressed (Figure 5d).

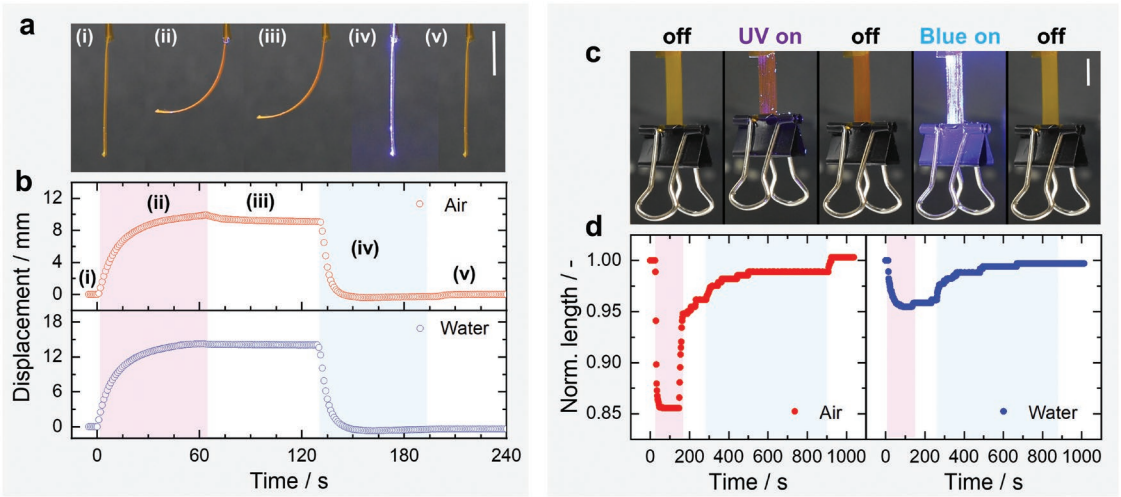

Figure 5. a) Photoactuation of the printed actuator without weight in air: i) prior to illumination; ii) UV light (25 mW cm^{-2}) illumination; iii) no UV light; iv) blue light (35 mW cm^{-2}) illumination; v) no blue light. The actuator is illuminated from the left. b) Tip displacement as a function of time in both air and water during UV (violet region) and blue (blue region) light illumination. The numbered regions correspond to the images in (a). c) Photoactuation of the printed actuator with load (1 g) in air using high-intensity UV (220 mW cm^{-2}) and blue (15 mW cm^{-2}) light. d) Normalized length (L/L_0) as a function of time in both air and water during UV (violet region) and blue (blue region) light illumination. The scale bars in (a) and (c) represent 0.5 cm.

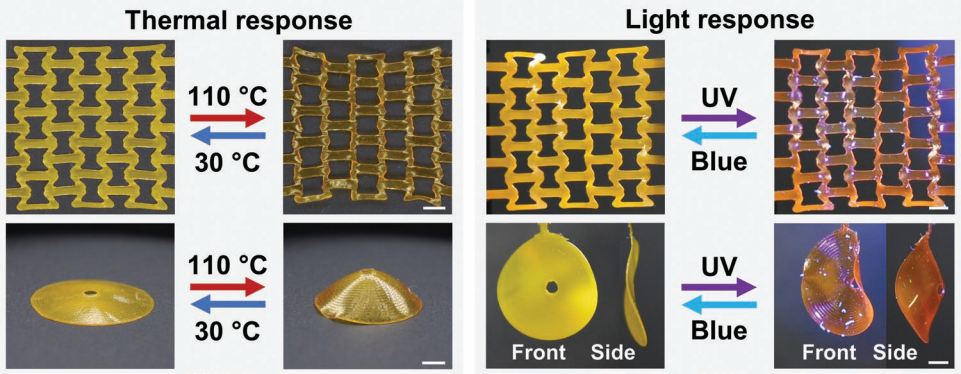

Figure 6. Reversible actuation of the complex re-entrant honeycomb (top) and spiral director (bottom) structures obtained by DIW in response to temperature (left) and light (right). The re-entrant honeycomb structure is fixed to a rigid frame (left and right sides of the structure in the photographs). The scale bars represent 0.25 cm.

When submerged in water, the printed actuator exhibits 4.5% contraction after illumination with high-intensity UV light (220 mW cm^{-2}) that is gradually completely recovered by exposure to blue light (15 mW cm^{-2}). Comparing the light-driven actuation in both surroundings shows that the degree of photochemical effects is similar (3.9% contraction), as expected. The actuator's specific work capacity was calculated for both surroundings with a maximum energy density of 2.4 J kg^{-1} in air and 0.5 J kg^{-1} in water (Supporting Information for details).

2.4. Temperature- and Light-Responsive Actuators with Programmed Structural Design

The versatility and design freedom provided by DIW is demonstrated by printing a porous re-entrant honeycomb structure and a spiral director orientation circular continuous layer, which show complex deformations in response to temperature and light (**Figure 6**).[33] Heating the auxetic honeycomb with fixed ends to 110 °C results in a structure with significant shape changes of the individual cells, and complete reversibility when cooled. The printed spiral director sample also exhibits a reversible response to temperature, allowing shape-morphing between the initial flat state and the actuated cone-like shape. In addition to the thermal response, light-responsive reversible actuation of the complex structures is also illustrated by exposure to UV (220 mW cm^{-2}) and blue light (15 mW cm^{-2}). Under UV illumination, both the re-entrant honeycomb and the spiral director structure undergo similar deformations as seen with thermal actuation, although to a lesser extent (Videos S4 and S5, Supporting Information). This reduced deformation is presumably due to inhomogeneous heating of the object during light-actuation and since only temperatures of 90 °C or lower are achieved (Figure S20, Supporting Information). Nevertheless, the light-driven actuation of these printed complex shapes is dominantly driven by thermal contributions as the deformation largely disappears when UV light is switched off. The remaining contraction based on the photochemical effect is recovered after illumination with blue light, which is similar to the printed actuator with load as discussed before. In the stripes and spiral director structure, the main deformation is bending, whereas the re-entrant honeycomb is fixed and limited to contraction and expansion that are less apparent as visualized by the changing angles of each unit cell. In addition, the molecular order of the stripe and spiral structure is higher than the re-entrant honeycomb, contributing to larger shape deformations (Figure S17, Supporting Information).

3. Conclusion

In conclusion, we have demonstrated the fabrication of light-responsive supramolecular LCEs for generating untethered soft actuators by 3D printing without the need for photocuring. Applying a thermoplastic polymer based on thermoreversible hydrogen bonds enables the facile printing of the molten material as viscoelastic ink, which subsequently solidifies on the printing bed into the polymer objects with molecular alignment. The photothermal and photochemical properties of the azobenzene moiety led to light-fueled soft actuators that can be operated both in air and aqueous environments with fast, reversible light-triggered macroscopic shape changes capable of lifting loads and performing mechanical work. Moreover, using DIW generates mesogen alignment while offering versatility in the structural design of the prints, enabling the generation of complex 3D objects and exotic deformation modes, as shown by printing re-entrant honeycomb and spiral director structures. This supramolecular material serves as an alternative approach for fabricating light-triggered LCE actuators via DIW. We believe that this thermoplastic, supramolecular design will open new routes to develop novel 3D-printed actuators, which can be used as 4D-printed soft robotics and deployable devices.

4. Experimental Section

Materials: Chemicals for the synthesis are: 1,4-Bis-[4-(3-acryloyloxypropyloxy)benzoyloxy]-2-methylbenzene (**1**, ≥97%) and 1,4-Bis-[4-(6-acryloyloxyhexyloxy)benzoyloxy]-2-methylbenzene (**2**, ≥97%) were purchased from Daken Chemical Ltd. 4,4-Bis-(6-acryloyloxyhexyloxy)azobenzene (**3**, ≥95%) was obtained from Synthon. Dimethylphenylphosphine (**5**, 99%) and *N*,*N*-Dimethylacetamide (DMAc, ≥99%) were obtained from Sigma-Aldrich. 2,2-(Ethylenedioxy) diethanethiol (**4**, ≥97%), Hexamethylene diisocyanate (**6**, ≥98%), Triethylamine (**7**, ≥99%), and 1,6-Hexanedithiol (**8**, ≥97%) were

purchased from Tokyo Chemical Industry (TCI). Diethyl ether (Et_2O, ≥99.5%) was obtained from Biosolve. For the preparation of sacrificial layers, poly(vinyl alcohol) (PVA; M_w 9000–10000, 80% hydrolyzed) was purchased from Sigma-Aldrich. All reagents were used as received without further purification.

Synthetic Procedure: The light-responsive PTU LCE was synthesized by charging a reaction vessel (250 mL) with diacrylate mesogens **1** (8.64 g, 14.67 mmol) and **2** (9.87 g, 14.67 mmol) and azobenzene **3** (1.38 g, 2.64 mmol) in DMAc (45 mL). After completely dissolving the monomers, dithiol **4** (7.00 g, 38.38 mmol) was added, followed by catalyst **5** (0.03 g, 0.19 mmol, 0.1 wt%) in DMAc (8 mL), and the reaction mixture was stirred under argon atmosphere at room temperature. After 2 h reaction time, diisocyanate **6** (2.15 g, 12.79 mmol) and catalyst **7** (0.03 g, 0.3 mmol, 0.1 wt%) were added to the mixture in DMAc (5 mL) and stirred at room temperature for 15 min. At this point, the viscosity increased and therefore additional DMAc (39 mL) was added. The reaction was continued by adding dithiol **8** (0.96 g, 6.40 mmol) in DMAc (3 mL) dropwise to the reaction mixture, after which it was allowed to stir at 60 °C overnight. The crude mixture was cooled to room temperature the next day, followed by precipitation into Et_2O (2 L) under continuous stirring. Afterward, the product was transferred into fresh Et_2O (500 mL) and stirred overnight. The final polymer was obtained by decanting the solvent and drying under a vacuum at 40 °C for 24 h yielding an orange solid (≥98% recovery).

General Characterizations: GPC was carried out using a Waters HPLC system equipped with a PSS PFG (8 × 50 mm^2, 7 µm) and two PFG linear XL columns (8 × 300 mm^2, 7 µm) in series. The samples were prepared in 1,1,3,3,3-hexafluoro-2-propanol (HFIP) with toluene (0.02 M) and potassium trifluoroacetate (0.02 M). HFIP with potassium trifluoroacetate (0.02 M) was supplied as a mobile phase at a flow rate of 0.8 mL min^{-1} at 35 °C. A refractive index detector was used to determine the molecular weight and dispersity relative to poly(methyl methacrylate). Attenuated total reflectance (ATR) and transmission FT-IR spectra were recorded on a Varian 670 IR spectrometer equipped with an ATR sampling accessory or a microscope setup and cross-polarizers. All spectra were taken with 50 scans over a range of 4000–650 cm^{-1} and a spectral resolution of 4 cm^{-1} at room temperature unless stated otherwise. The FT-IR spectra obtained were processed with Varian Resolutions and SpectraGryph. UV–vis spectrophotometry was recorded on a PerkinElmer Lambda 750 spectrophotometer equipped with an integrating sphere detector, a tungsten halogen light source, and an automatic polarizer for polarized absorption experiments. Measurements were performed on drop-cast samples (T = 1.5 µm) from HFIP (10 mg mL^{-1}) placed in front of the integrating sphere. NMR spectra were recorded at room temperature on a Bruker Avance III HD NanoBay 400 MHz in $CDCl_3$/HFIP (95/5% v/v). Chemical shifts are with respect to tetramethylsilane (TMS, 0 ppm) in $CDCl_3$ (purchased from Sigma-Aldrich, 0.03% v/v TMS, 99.8 atom% D). DSC scans were collected using a TA Instruments Q2000 DSC instrument equipped with a cooling accessory between −50 and 210 °C at 10 °C min^{-1} under nitrogen. The measurement was performed in a hermetic T-zero aluminum sample pan with 10 mg product, and the transition temperatures were determined from the second cycle. TGA was performed on a TA instruments Q50 instrument between 28 and 800 °C at 5 °C min^{-1} with 4 mg product. Thermomechanical characterization (E′, E″, and loss tangent) was carried out with DMA on compression-molded samples (8.9 × 5.5 × 1.1 mm^3) using a TA Instruments Q800 apparatus in vertical tension mode. Thermographs were obtained between −50 and 200 °C at a heating rate of 5 °C min^{-1} with 0.01 N preload force, 12 µm amplitude, and a single 1 Hz oscillating frequency. Thermal stress relaxation and iso-stress measurements were also performed with DMA on compression-molded films (8.0 × 5.3 × 0.3 mm^3). For stress relaxation, the samples were equilibrated for 5 min at each temperature (100–150 °C) and subsequently strained to ε = 100%. For iso-stress, the samples were subjected to a constant force (σ = 10 kPa) and a temperature ramp of 5 °C min^{-1}. The stress–strain curve was measured using a Lloyd-Ametek EZ20 tensile testing machine equipped with a 500 N load cell on compression-molded dog-bone specimens (2 × 0.4 mm^2) with a 20 mm gauge length and 10 mm min^{-1} elongation rate until failure. The strain is defined as (l–L)/L, where L is the initial length and l at a certain time. POM images were recorded with a Leica DM2700 M microscope equipped with cross-polarizers and a Leica MC170 HD camera. The isotropization temperature was obtained from drop-cast samples (15 mg mL^{-1} in HFIP) using a Linkam THMS600 heating and cooling unit with a 10 °C min^{-1} rate. WAXS and MAXS measurements were performed on a Ganesha lab instrument equipped with a Genix-Cu ultralow divergence source (Cu Kα, λ = 0.154 nm, $\Phi = 1 \times 10^8$ photons s^{-1}) and a Pilatus 300 K silicon pixel detector (487 × 619 pixels, 172 µm^2 in size), placed at a sample-to-detector distance of 89 mm (WAXS) or 440 mm (MAXS). Diffraction patterns were collected with an exposure time of 30 min (WAXS) or 60 min (MAXS) and analyzed using a custom Python script with the PyFAI software package. Silver behenate was used as the calibration standard. The orientational order parameter S was determined using the Kratky method.[57] Photographs and videos were taken with a camera (Olympus OM-D E-M10 Mark III or Nikon D3300) in manual mode.

Fabrication of Mechanically Programmed Actuators: The polymer was cut into small pieces and dried at 80 °C under vacuum for 1 h. It was then homogeneously loaded into a metal mold (20 × 40 × 0.1 mm^3) and covered with polytetrafluoroethylene sheets on both sides. Compression-molded samples were obtained using a Collin P200E press at 200 °C by first performing three degassing cycles at a pressure of 50 bar, followed by a final molding cycle at 100 bar. After 2 min, the mold was quenched to room temperature by flowing water through it yielding polymer films (20 × 40 × 0.3 mm^3). Next, small stripes of material (20 × 3 × 0.3 mm^3) were cut from the resulting film and stretched to ε = 200% at room temperature using a custom-made stretching device, which were then heated to 130 °C for 30 min. After this, the samples were allowed to cool to room temperature and stored at ambient conditions for at least 48 h prior to testing.

Direct Ink Writing of the Supramolecular LCE Actuators: A GESIM BioScaffolder 3.2 equipped with a high-temperature piston extruder and 300 µm metal nozzle was used for printing the supramolecular LCE. First, the polymeric material was dried at 80 °C under vacuum for 90 min and subsequently loaded into the printhead at room temperature. To obtain a homogenous thermoplastic polymer melt as ink for DIW, the material was heated to 200 °C for 15 min. For printing, the temperature of the nozzle was decreased to 180 °C and for the printhead even further to 175 °C, while the printing bed was maintained at room temperature. The piston feed ranged between 1 and 5 µm s^{-1} and the printing speed between 3 and 10 mm s^{-1}. The layer height was set to 0.05 mm and the line spacing to 0.3 mm. DIW was performed on conventional glass microscope slides coated with a sacrificial PVA layer for easy sample release to yield free-standing prints. With spin-coating (1800 rpm for 60 s), a 5 wt% PVA solution in Milli-Q purified water was cast on the glass slides and then dried at 60 °C for 60 min. The computer-aided design (CAD) files were prepared in Libre-Cad freeware software, 3D builder from Microsoft, and GeSiM Robotics software, in which the DIW was reconfigured and controlled according to the chosen settings. Films (15 × 3 mm^2) or more complex shapes were printed on the PVA-coated glass substrates, which were then submerged in water to dissolve the sacrificial layer and dried at room temperature to obtain free-standing actuators. The sample thickness of the prints was measured using a profilometer and ranged between 93 and 118 µm.

Thermal Actuation: The mechanically programmed and direct ink written actuators were placed on a black aluminum plate (T = 0.01 mm) on top of a heating and cooling stage (Linkam THMS600). Prior to the actuation measurements, the thermal history was erased by subjecting all samples to a full heating and cooling cycle. The samples were heated and cooled between 30 and 110 °C with temperature intervals of 10 °C. Images were analyzed using ImageJ. LEDs provided lighting in a photo box. For the re-entrant honeycomb structure, the sample was fixed at the two ends to the substrate with tape.

Light Actuation in Air and Underwater: Light-driven actuation of the mechanically programmed actuator was performed by hanging the aligned film (19 × 2 × 0.2 mm^3) at a 10 cm distance from the

collimated light sources with light-emitting at 365 nm (UV light, Thorlabs M365L2) or 455 nm (Blue light, Thorlabs M455L3-C2). The light intensity of the LEDs was controlled using a LED driver (Thorlabs DC4104). The illumination time and interval in between and after was 30 s for actuation in both surroundings. Photoactuation in air was performed at room temperature with UV and blue light intensities set to 25 and 35 mW cm^{-2}, respectively. For underwater photoacutation, the sample was submerged in a transparent glass container filled with tap water at room temperature and illuminated with UV and blue light with intensities of 20 and 29 mW cm^{-2}, respectively. For the samples fabricated by DIW, the stripes and spiral were fixed at the upper end, while the re-entrant honeycomb structure was fixed at two sides to a frame. Bending experiments in air (365 nm: 25 mW cm^{-2}, 455 nm: 35 mW cm^{-2}) and underwater (365 nm: 24 mW cm^{-2}, 455 nm: 33 mW cm^{-2}) of the printed stripes were performed without load, while for the contraction experiments in both surroundings (365 nm: 220 mW cm^{-2}, 455 nm: 15 mW cm^{-2}), a weight of 1 g was attached to the lower end. Photoactuation in air was performed with a custom-made metal structure to fix the sample. A metallic camber with two opposing glass plates or a transparent glass container containing water was used for underwater actuation. The illumination time and interval were 1 min for the bending experiments. The contraction experiments with load were performed with 2 min illumination UV light and 10 min blue light with 2 min interval. Thermography images and temperature profiles of the photoactuation in air were recorded with a thermographic camera (Xenics Gobi). All samples were subjected to several actuation cycles with the corresponding conditions to verify the reversibility and reproducibility of the shape changes before the photoactuation experiments. Analysis of the bending and contraction experiments was performed with ImageJ software on images extracted from the videos. For photoactuation with load, the length of the samples was measured between the bottom end of the Kapton tape and the top end of the weight. It should be noted that samples without azobenzene **3** do not show shape changes upon illumination with UV and blue light.

Supporting Information

Supporting Information is available from the Wiley Online Library or from the author.

Acknowledgements

The authors sincerely thank Nico van Rijswijk for his contribution to the experimental work, Dr. Marc del Pozo for help with the light-responsive actuation, Dr. Jeroen Sol for the discussion regarding direct ink writing, and Dr. Michael Debije for his careful reading of the manuscript. They also thank PRIME and SFD colleagues for their valuable suggestions and discussions. The described research study is part of the project PRIME. This work was funded by the European Union's Horizon 2020 Research and Innovation Programme under grant agreement no. 829010 (PRIME). Funding has also been received from Spanish "Ministerio de Ciencia, Innovación y Universidades (MCIU)" through AEI/FEDER(UE) PID2020-118485RB-I00 project, FEDER (EU) and Fondo Social Europeo (DGA E47_20R).

Conflict of Interest

The authors declare no conflict of interest.

Author Contributions

The manuscript was written with the contributions of all authors. All authors have given approval to the final version of the manuscript.

Data Availability Statement

The data that support the findings of this study are available from the corresponding author upon reasonable request.

Keywords

azobenzene, direct ink writing, light-responsive polymer, liquid crystals, soft actuators, supramolecular polymer, 4d printing

Received: September 6, 2022
Published online: December 25, 2022

[1] X. Pang, J. Lv, C. Zhu, L. Qin, Y. Yu, *Adv. Mater.* **2019**, *31*, 1904224.
[2] J. M. McCracken, B. R. Donovan, T. J. White, *Adv. Mater.* **2020**, *32*, 1906564.
[3] M. Pilz da Cunha, Y. Foelen, R. J. H. van Raak, J. N. Murphy, T. A. P. Engels, M. G. Debije, A. P. H. J. Schenning, *Adv. Opt. Mater.* **2019**, *7*, 1801643.
[4] S. Huang, Y. Huang, Q. Li, *Small Struct.* **2021**, *2*, 2100038.
[5] L. Hines, K. Petersen, Z. Lum, M. Sitti, L. Hines, G. Z. Lum, M. Sitti, K. Petersen, *Adv. Mater.* **2017**, *29*, 1603483.
[6] S. I. Rich, R. J. Wood, C. Majidi, *Nat. Electron.* **2018**, *1*, 102.
[7] M. Pilz Da Cunha, M. G. Debije, A. P. H. J. Schenning, *Chem. Soc. Rev.* **2020**, *49*, 6568.
[8] M. Rogóż, H. Zeng, C. Xuan, D. S. Wiersma, P. Wasylczyk, *Adv. Opt. Mater.* **2016**, *4*, 1689.
[9] J. A. Lv, Y. Liu, J. Wei, E. Chen, L. Qin, Y. Yu, *Nature* **2016**, *537*, 179.
[10] O. M. Wani, H. Zeng, A. Priimagi, *Nat. Commun.* **2017**, *8*, 1.
[11] G. Stoychev, A. Kirillova, L. Ionov, *Adv. Opt. Mater.* **2019**, *7*, 1900067.
[12] J. Gao, M. Tian, Y. He, H. Yi, J. Guo, *Adv. Funct. Mater.* **2022**, *32*, 2107145.
[13] S. Nocentini, C. Parmeggiani, D. Martella, D. S. Wiersma, *Adv. Opt. Mater.* **2018**, *6*, 1800207.
[14] H. Zeng, P. Wasylczyk, D. S. Wiersma, A. Priimagi, *Adv. Mater.* **2018**, *30*, 1703554.
[15] W. Wei, Z. Zhang, J. Wei, X. Li, J. Guo, *Adv. Opt. Mater.* **2018**, *6*, 1800131.
[16] L. Dong, Y. Zhao, *Mater. Chem. Front.* **2018**, *2*, 1932.
[17] T. J. White, *J. Polym. Sci., Part B: Polym. Phys.* **2018**, *56*, 695.
[18] Z. C. Jiang, Y. Y. Xiao, Y. Zhao, *Adv. Opt. Mater.* **2019**, *7*, 1900262.
[19] H. K. Bisoyi, Q. Li, *Chem. Rev.* **2016**, *116*, 15089.
[20] M. Pilz Da Cunha, E. A. J. Van Thoor, M. G. Debije, D. J. Broer, A. P. H. J. Schenning, *J. Mater. Chem. C* **2019**, *7*, 13502.
[21] A. Priimagi, A. Shimamura, M. Kondo, T. Hiraoka, S. Kubo, J. I. Mamiya, M. Kinoshita, T. Ikeda, A. Shishido, *ACS Macro Lett.* **2012**, *1*, 96.
[22] S. K. Ahn, T. H. Ware, K. M. Lee, V. P. Tondiglia, T. J. White, *Adv. Funct. Mater.* **2016**, *26*, 5819.
[23] J. Sun, B. Peng, Y. Lu, X. Zhang, J. Wei, C. Zhu, Y. Yu, *Small* **2022**, *18*, 2106443.
[24] C. Chen, Y. Liu, X. He, H. Li, Y. Chen, Y. Wei, Y. Zhao, Y. Ma, Z. Chen, X. Zheng, H. Liu, *Chem. Mater.* **2021**, *33*, 987.
[25] J. H. Lee, J. Bae, J. H. Hwang, M. Y. Choi, Y. S. Kim, S. Park, J. H. Na, D. G. Kim, S. kyun Ahn, *Adv. Funct. Mater.* **2022**, *32*, 2110360.
[26] Y. Zhou, L. Wang, S. Ma, H. Zhang, *ACS Appl. Mater. Interfaces* **2022**, *14*, 3264.
[27] T. Ube, R. Nakayama, T. Ikeda, *Macromolecules* **2022**, *55*, 413.
[28] W. Shen, J. Liu, B. Du, H. Zhuo, S. Chen, *J. Mater. Chem. A* **2021**, *9*, 15087.
[29] W. Shen, B. Du, J. Liu, H. Zhuo, C. Yang, S. Chen, *Mater. Chem. Front.* **2021**, *5*, 3192.

[30] X. Wan, L. Luo, Y. Liu, J. Leng, *Adv. Sci.* **2020**, *7*, 2001000.
[31] Z. Wang, Y. Guo, S. Cai, J. Yang, *ACS Appl. Polym. Mater.* **2021**, *4*, 3153.
[32] J. A. H. P. Sol, L. G. Smits, A. P. H. J. Schenning, M. G. Debije, *Adv. Funct. Mater.* **2022**, *32*, 2201766.
[33] M. López-Valdeolivas, D. Liu, D. J. Broer, C. Sánchez-Somolinos, *Macromol. Rapid Commun.* **2018**, *39*, 1700710.
[34] C. P. Ambulo, J. J. Burroughs, J. M. Boothby, H. Kim, M. R. Shankar, T. H. Ware, *ACS Appl. Mater. Interfaces* **2017**, *9*, 37332.
[35] A. Kotikian, R. L. Truby, J. W. Boley, T. J. White, J. A. Lewis, *Adv. Mater.* **2018**, *30*, 1706164.
[36] H. K. Bisoyi, Q. Li, *Chem. Rev.* **2022**, *122*, 4887.
[37] L. Ceamanos, Z. Kahveci, M. Lopez-Valdeolivas, D. Liu, D. J. Broer, C. Sanchez-Somolinos, *ACS Appl. Mater. Interfaces* **2020**, *12*, 44195.
[38] M. del Pozo, L. Liu, M. Pilz da Cunha, D. J. Broer, A. P. H. J. Schenning, *Adv. Funct. Mater.* **2020**, *30*, 2005560.
[39] M. del Pozo, J. A. H. P. Sol, S. H. P. Van Uden, A. R. Peeketi, S. J. D. Lugger, R. K. Annabattula, A. P. H. J. Schenning, M. G. Debije, *ACS Appl. Mater. Interfaces* **2021**, *13*, 59381.
[40] X. Lu, C. P. Ambulo, S. Wang, L. K. Rivera-Tarazona, H. Kim, K. Searles, T. H. Ware, *Angew. Chem., Int. Ed* **2021**, *60*, e202202577.
[41] S. J. D. Lugger, R. M. C. Verbroekken, D. J. Mulder, A. P. H. J. Schenning, *ACS Macro Lett.* **2022**, *11*, 935.
[42] S. J. D. Lugger, D. J. Mulder, A. P. H. J. Schenning, *Angew. Chem., Int. Ed* **2022**, *61*, e202115166.
[43] N. G. Ireni, M. Karuppaiah, R. Narayan, K. V. S. N. Raju, P. Basak, *Polymer* **2017**, *119*, 142.
[44] K. Gu, J. Onorato, S. S. Xiao, C. K. Luscombe, Y. L. Loo, *Chem. Mater.* **2018**, *30*, 570.
[45] N. G. Ireni, R. Narayan, P. Basak, K. V. S. N. Raju, *Polymer* **2016**, *97*, 370.
[46] K. Kojio, M. Furukawa, S. Motokucho, M. Shimada, M. Sakai, *Macromolecules* **2009**, *42*, 8322.
[47] A. Takahara, J. Tashita, T. Kajiyama, M. Takayanagi, *J. Biomed. Mater. Res.* **1985**, *19*, 13.
[48] E. Anglaret, M. Brunet, B. Desbat, P. Keller, T. Buffeteau, *Macromolecules* **2005**, *38*, 4799.
[49] M. Dai, O. T. Picot, J. M. N. Verjans, L. T. De Haan, A. P. H. J. Schenning, T. Peijs, C. W. M. Bastiaansen, *ACS Appl. Mater. Interfaces* **2013**, *5*, 4945.
[50] J. Lub, D. J. Broer, R. T. Wegh, E. Peeters, B. M. I. Van Der Zande, *Mol. Cryst. Liq. Cryst.* **2005**, *429*, 77.
[51] S. Sakurai, H. Yoshida, F. Hashimoto, M. Shibaya, H. Ishihara, N. Yoshihara, S. Nishitsuji, M. Takenaka, *Polymer* **2009**, *50*, 1566.
[52] R. W. Seymour, A. E. Allegrezza, S. L. Cooper, *Macromolecules* **1973**, *6*, 896.
[53] Z. Wen, M. K. McBride, X. Zhang, X. Han, A. M. Martinez, R. Shao, C. Zhu, R. Visvanathan, N. A. Clark, Y. Wang, K. Yang, C. N. Bowman, *Macromolecules* **2018**, *51*, 5812.
[54] A. Gablier, M. O. Saed, E. M. Terentjev, *Macromolecules* **2020**, *53*, 8642.
[55] D. Dattler, G. Fuks, J. Heiser, E. Moulin, A. Perrot, X. Yao, N. Giuseppone, *Chem. Rev.* **2020**, *120*, 310.
[56] M. del Pozo, J. A. H. P. Sol, A. P. H. J. Schenning, M. G. Debije, *Adv. Mater.* **2022**, *34*, 2104390.
[57] M. T. Sims, L. C. Abbott, R. M. Richardson, J. W. Goodby, J. N. Moore, *Liq. Cryst.* **2019**, *46*, 11.